Application of MTO Thyristors in Current Stiff Converters with Resonant Snubbers

Braz J. Cardoso Filho, *Member, IEEE,* and Thomas A. Lipo, *Fellow, IEEE*

***Abstract*—This paper addresses the impact of power devices switching characteristics on design and performance of pulsewidth-modulated current stiff converter (CSC) topologies with resonant snubbers. The MOS turn-off (MTO) thyristors were selected for this study due to their high voltage and current ratings, simplified gate drive circuitry, unity gain turn-off, greatly reduced storage time allowing higher switching frequencies, and reverse voltage blocking capability. The analysis presented in this paper is supported by experimental data obtained from a CSC commutation cell capable of reproducing all the commutation processes in the current stiff converter topologies with active resonant snubbers. Issues involved in the implementation of the commutation cell itself and MTO characteristics relevant for their operation in CSC topologies with resonant snubbers are addressed in detail in this paper.**

***Index Terms*—Current stiff inverter, MOS turn-off thyristor, resonant snubber, soft switching.**

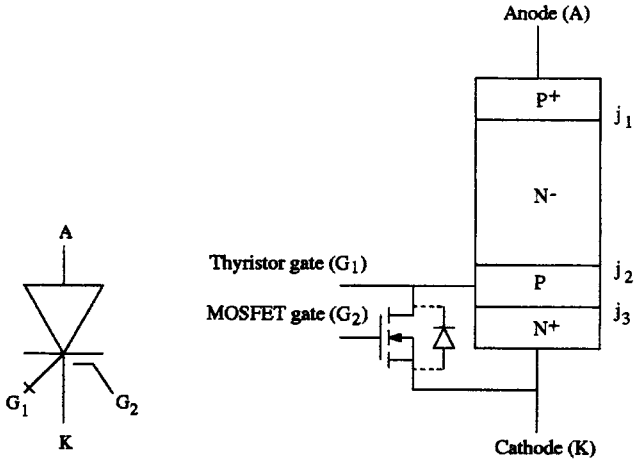

Fig. 1. MTO thyristor.

I. Introduction

RESONANT snubbers [1] have recently been proposed for improvement of the performance of pulsewidth-modulated (PWM) current stiff converters (CSCs) [2]–[4]. Among the advantages of resonant snubbers when compared to classical *LRCD* snubbers [5] and regenerative schemes [6], one can point out: essentially lossless structure, intrinsic minimization of stray inductances improving device utilization, and reasonably low parts count and hardware complexity. On the other hand, resonant snubbers are active circuits and require control for proper operation.

Resonant snubber design goals are minimization of the switching losses while constraining voltage and current stresses on the main switches and snubber components. The design of the resonant snubber components is then greatly dependent on the switching characteristics of the main power devices employed in the CSC. In this paper, high-power MOS turn-off (MTO) thyristors [7] were investigated for application in CSC topologies with resonant snubbers. These new devices present improved turn-off characteristics, simplified gate drive requirements, unity gain turn-off, short storage time ($\approx$1 μs) and reverse voltage blocking capability. Other high-power devices such as the integrated gate controlled thyristors (IGCTs) and high-voltage insulated gate bipolar transistors (HV-IGBTs) are also interesting possibilities, mainly if a series diode is introduced in the device package to add reverse voltage blocking capability.

The analysis presented in this paper is supported by experimental results obtained from a commutation cell capable of reproducing all the commutation processes corresponding to current stiff converter topologies with resonant snubbers [1]–[4]. This commutation cell is based on the MTO XSDM170HK (4500 V/500 A) [8]. Issues involved in the implementation of the commutation cell itself as well as the MTO-thyristor characteristics relevant for the operation in CSC topologies with resonant snubbers are addressed in detail in this paper.

Paper IPCSD 00–054, presented at the 1999 Industry Applications Society Annual Meeting, Phoenix, AZ, October 3–7, and approved for publication in the IEEE TRANSACTIONS ON INDUSTRY APPLICATIONS by the Industrial Power Converter Committee of the IEEE Industry Applications Society. Manuscript submitted for review August 1, 2000 and released for publication November 26, 2000.

B. J. Cardoso Filho is with the Departamento Engenharia Eletrica, Universidade Federal de Minas Gerais, Belo Horizonte 31270-010, Brazil (e-mail: cardosob@cpdee.ufmg.br).

T. A. Lipo is with the Department of Electrical and Computer Engineering, University of Wisconsin Madison, WI 53706 USA (e-mail: lipo@engr.wisc.edu).

Publisher Item Identifier S 0093-9994(01)02105-3.

II. Overview of MTO-Thyristor Characteristics

A. Forward Bias

The MTO gate-turn-off process is based on the introduction of a very low impedance ($r_{DS_{\mathrm{on}},eq}$ of the MOSFETs in the device) in parallel with the junction j_3, as shown in Fig. 1. With the MOSFETs on, the gate current increases rapidly in the negative direction. Almost all of the load current is transferred to the MOSFETs since the voltage drop across them at a given current is much lower than the voltage across junction j_3 [7]. The

injection of electrons from the N^+ emitter into the P-base is suppressed and the p-n-p transistor in the MTO structure enters an open-base turn-off process. In fact, the MTO structure in the off state is similar to that of regular thyristors with emitter shorts.

The MTO dV/dt capability is also a function of the total gate–cathode resistance in the off state. Low equivalent P-base and on-state MOSFET resistances are required to prevent the displacement current associated with the change in the width of the drift region to forward bias junction j_3 and trigger the device into conduction (particularly important at high forward blocking voltages).

The situations pointed out above imply a fairly low $r_{P\text{-base},eq}$ in the MTO thyristors, yielding a low gate–cathode resistance in the off-state. However, a reduction in the equivalent P-base resistance degrades the on-state characteristics of the device. Larger front-porch and back-porch gate current requirements are expected as a result of low $r_{P-\text{base},eq}$ [9].

The voltage driving the negative gate current in the MTOs during the turn-off process is the voltage across the gate–cathode junction of the thyristor part of the device (V_{bi}) [10]. This low driving voltage combined to stray inductances in the turn-off path of the gate current increase the chances for nonhomogeneous turn-off, particularly at higher anode currents, and nonuniform current sharing among the multiple MOSFETs. Uniform pressure over the entire device surface is expected to be even more critical in the MTOs than in regular gate-turn-off thyristors (GTOs) for uniform turn-off.

B. Reverse Bias

MTOs are switched from the conduction mode to the reverse blocking mode by negative anode voltage, through a zero-current turn-off process similar to that observed in regular thyristor devices. However, the intrisic reverse diodes across the turn-off MOSFETs in the MTO structure constrain the reverse voltage across junction j_3, such that $v_{j_3} > 0$. As a result, no reverse voltage breakdown takes place across junction j_3.

Under negative anode voltage, both p-n-p and n-p-n transistors in the device structure operate in the reverse bias mode. This situation implies that the MTO does not latch up under reverse anode voltage if positive current is injected into the turn-on gate terminal G_1, with junctions j_2 and j_3 forward biased. Injection of current into G_1 leads to an increase of the reverse anode current. The device operates in the remote base transistor mode (active region) [11]. In this operating mode, the current gain $|i_A|/i_{G_1}$ is quite low, increasing in direct proportion to the anode voltage (the equivalent base transport factor rises as the width of the neutral region in the N-base is reduced).

III. Commutation in CSC Topologies with Resonant Snubbers

A. Realization and Commutation Sequences [2]

The basic implementation of the resonant snubbers with auxiliary switches for CSCs is depicted in Fig. 2 [1]. The CSC realization requires one auxiliary device for each pair of main switches in the common-anode and common-cathode groups. A back-to-back arrangement of snubber devices, as in the voltage stiff converter (VSC) [1], [12] realization, can also be used to minimize the influence of the dc-bus current on the commutation process.

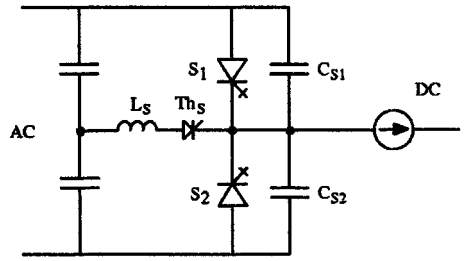

Fig. 2. Basic realizations of the resonant snubbers in CSC.

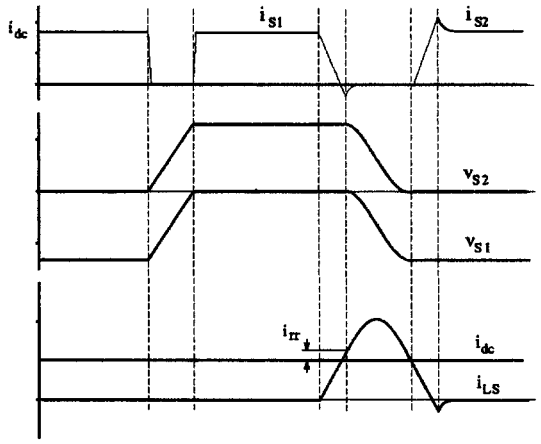

Fig. 3. Basic waveforms of the CSC with resonant snubbers.

Fig. 3 shows the relevant waveforms of the resonant snubber implementation in CSCs, where two commutation sequences can be identified. The *passive commutation sequence* takes place whenever the incoming switch is reverse biased. Otherwise, external means have to be provided to establish zero-voltage conditions on the incoming switch during its turn-on process and the *active commutation sequence* takes place.

The passive commutation sequence starts when the conducting switch is turned off. The dc-bus current commutates to the snubber capacitors and the voltage across the devices ramps up. The incoming switch starts conducting at the zero crossing of the voltage across its terminals.

The active commutation sequence is based on the introduction of a resonant mode to drive the voltage across the incoming switch down to zero. This sequence starts by turning on the snubber switch. The current through the snubber inductor ramps up, reaching the dc bus current amplitude. At this instant, the outgoing switch is turned off under zero-current conditions. Since no switch is conducting, a resonant mode between the snubber inductor and capacitors takes place. The charge in the snubber capacitor across the incoming switch is transferred to the one across the outgoing switch (reverse biased) and the incoming switch turns on under zero anode voltage.

B. Test Setup

The high-power (pulsed) test setup implemented for the evaluation of the resonant snubbers in CSC topologies is depicted

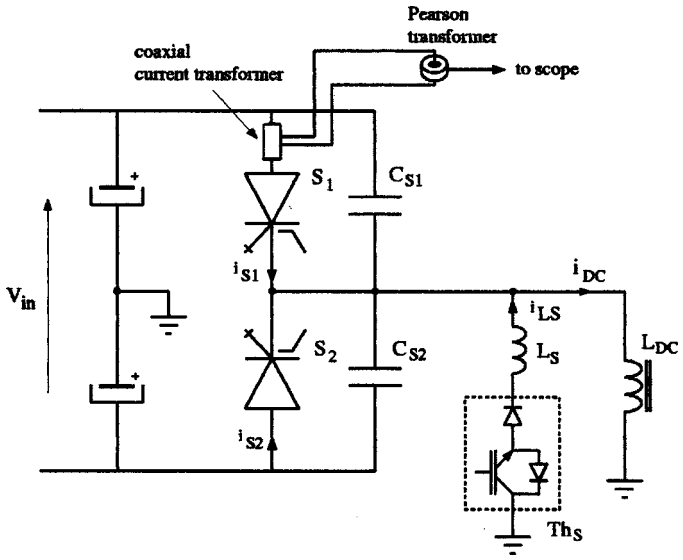

Fig. 4. High-power (pulsed) test setup employing MTOs.

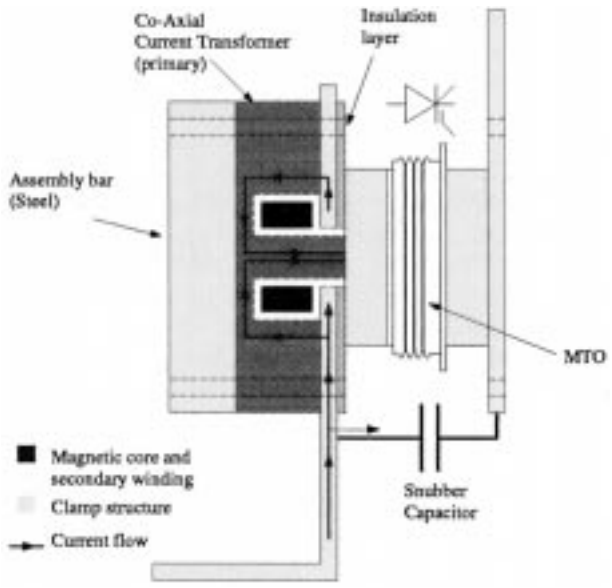

Fig. 5. Detail of the assembly of the coaxial current transformer.

in Fig. 4, with MTO devices employed in the main switches (S_1 and S_2). A series-connected IGBT and fast-recovery diode set is employed as the snubber switch (Th_S).

The test circuit in Fig. 4 is capable of reproducing both passive and active commutation sequences with minimum hardware and control complexity. In this circuit, the snubber driving voltage is set for *optimal* commutation conditions [2] with the snubber driving voltage derived from the center tap of the input supply $V_{\rm in}$. *Near optimal* commutation conditions [3] can be set by introducing an independent supply to set the snubber driving voltage or by splitting the input voltage in multiple levels.

A cascade connection of two current transformers has been used to minimize the total insertion impedance associated with the measurement of the current through the devices. A coaxial current transformer was inserted directly in the power setup. This transformer employs a wound-tape toroidal core (part number W783 50 451-1/2D from MAGNETICS). The secondary winding consists of ten turns of copper tape wound around the toroidal core. The primary side of the transformer was built by machining a toroidal shape with the proper dimensions to accomodate the transformer core and secondary winding in a copper bar. Fig. 5 shows a detail of the power setup illustrating the connection of the primary side of the coaxial current transformer to the power device. Notice that this arrangement allows the measurement of the current through the power device only and does not include the snubber capacitor current. The current through the shorted secondary winding of the coaxial transformer is then measured using a commercial current transformer (PEARSON 411). The total gain of the cascade connection is 0.01 V/A (1-MΩ input impedance).

The operation of the test setup is illustrated by the idealized waveforms depicted in Fig. 6. Passive commutation processes take place at instants t_1 and t_3. Active commutation process is observed at instant t_2. Fig. 6 also shows the commands for all the switches in the circuit.

The commutation cell described here was tested for several values of dc-bus current, input voltage, and snubber capacitor values in order to identify tradeoffs in CSC operation involving

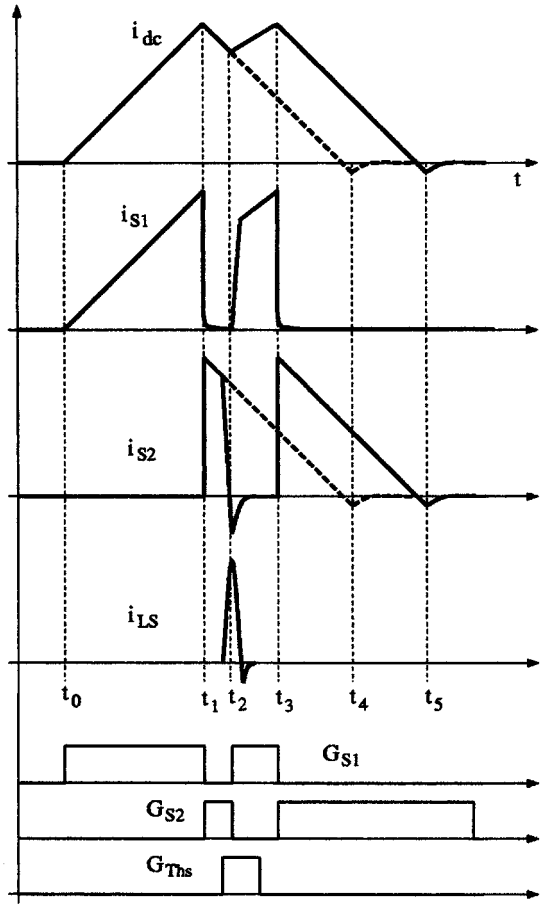

Fig. 6. High-power (pulsed) test setup main waveforms.

these quantities. The following paragraphs present the procedures and summarize the results obtained in this investigation.

C. Passive Commutation

Typical passive commutation waveforms illustrating the entire switching transient are shown in Fig. 7, where commutation

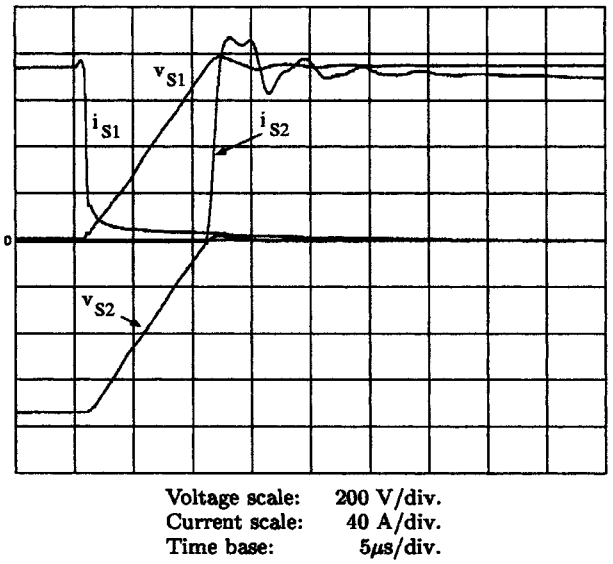

Fig. 7. Passive commutation sequence.

takes place from switch S_1 to switch S_2. These plots were obtained with $i_{\rm dc} = 150$ A, $V_{\rm in} = 750$ V, and $C_S = 1.0\,\mu$F. While the turn-off process is similar to that observed in VSC topologies, the turn-on process implies reverse bias on the incoming switch and it is proper of CSC topologies employing self-commutated devices.

1) Turn-Off Process Issues: The turn-off loss in the passive commutation sequence is the main figure in the design of the snubber capacitors. The lossless reset mechanism provided by the resonant snubber allows the use of larger snubber capacitors than in classical *LRCD* snubbers, leading to significant reduction of the turn-off loss and better device utilization.

In Fig. 7 the dV/dt across the device is about 75 V/μs. The voltage spike (and related power dissipation spike) across the device due to the stray inductances in the switch–snubber capacitor loop has been greatly reduced. The voltage overshoot shown in this figure is the voltage transient across the incoming switch due to combined effects of series stray inductance and the forward recovery process (significantly lower than the input voltage). The anode current peaking shown in Fig. 7 has been observed and described earlier in the literature for GTO thyristors in resonant dc-link converters [13]. The anode peaking phenomenon was explained as being caused by stray inductances causing transients in the anode–cathode voltage as the gate–cathode junction recovers its voltage blocking capability. Relevant turn-off data is summarized in Table I.

2) Turn-On Process Issues: The incoming switch S_2 enters conduction as soon as $v_{AK} > 0$. The overshoot in the current through S_2 is due to the stray inductance in series with the device and its forward recovery process (voltage overshoot followed by discharge of the snubber capacitor through the device).

The incoming switch is expected to start conducting at the zero crossing point of its anode–cathode voltage, provided that turn-on gate signals are supplied at a proper time. In this sense, it is desirable to apply the turn-on gate command to the incoming switch in advance, anticipating the zero crossing instant and minimizing the forward recovery losses. Positive current injection in gate G_1 while the MTO is still reverse biased takes the device into the far base transistor mode, operating in the active region. The current gain $|i_A|/i_{G_1}$ is strongly influenced by the anode voltage, that affects directly the N-base width and the p-n-p transistor base transport factor (Early effect).

TABLE I
PASSIVE COMMUTATION—TURN-OFF DATA SUMMARY

C_S [μF]	i_{dc} [A]	V_{in} [V]	E_{off} [mJ]	$t_{storage}$ [μs]	t_{fall} [μs]	$v_{ak_{max}}/V_{in}$ [V/V]
0.47	100	750	56	1.1	0.31	1.06
1.0	100	750	41	1.0	0.32	1.04
1.0	150	750	77	1.0	0.22	1.05
1.0	200	750	90	0.9	0.19	1.08

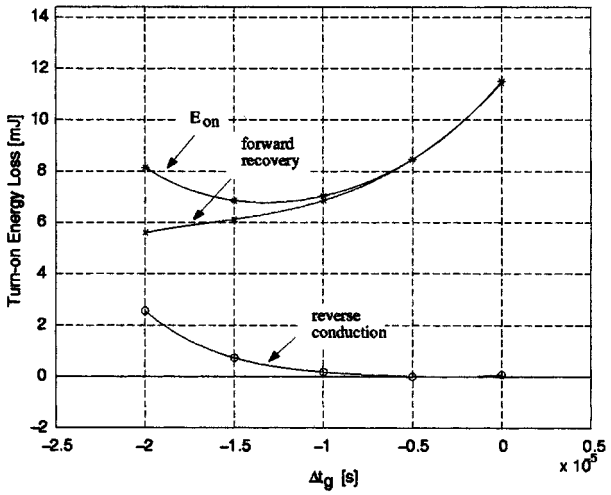

Fig. 8. Passive commutation: turn-on energy loss.

The effect of the anode voltage amplitude on the gain $|i_A|/i_{G_1}$ and the dynamics of the resonant snubber point out the trigger delay between the gate turn-on command of the incoming switch and the gate turn-off command of the outgoing switch, $\Delta t_g = t_{g,\,\rm on} - t_{g,\,\rm off}$, as a manipulation parameter to minimize the turn-on losses on the incoming switch due to transistor action and the forward recovery process. These energy loss terms as well as the total turn-on losses are shown in Fig. 8, for $V_{\rm in} = 600$ V, $i_{\rm dc} = 100$ A, and $C_S = 1\,\mu$F as a function of Δt_g. A minimum turn-on energy point exists for given switching conditions. The dependence of the turn-on losses due to transistor action on the reverse anode voltage and considerations regarding simplification on the trigger timing and control logic suggest $\Delta t_g = 0$ as the standard trigger delay.

A summary of relevant turn-on data obtained from the MTO-based test setup is listed in Table II ($\Delta t_g = 0$). The di_A/dt data in Table II has been evaluated at the point where $i_A = i_{\rm dc}/2$.

It has been pointed out in the literature that the lack of a series inductor to limit the di_A/dt during the passive commutation sequence would limit the applicability of this snubber structure in converter circuits based on thyristor-type devices [6]. However, the di_A/dt data in Table II do not support the position above. In fact, the tests confirm the self-limited di_A/dt characteristic of the MTO and, by extension, of GTO devices at turn-on, as pointed out by Wood [14]. The conclusion in

TABLE II
PASSIVE COMMUTATION—TURN-ON DATA SUMMARY

C_S [μF]	i_{dc} [A]	V_{in} [V]	E_{on} [mJ]	di_A/dt [A/μs]	$i_{A,max}/i_{dc}$ [A/A]
0.47	100	750	3	139	1.20
1.0	100	750	3	118	1.19
1.0	150	750	13	168	1.17
1.0	200	750	29	188	1.21

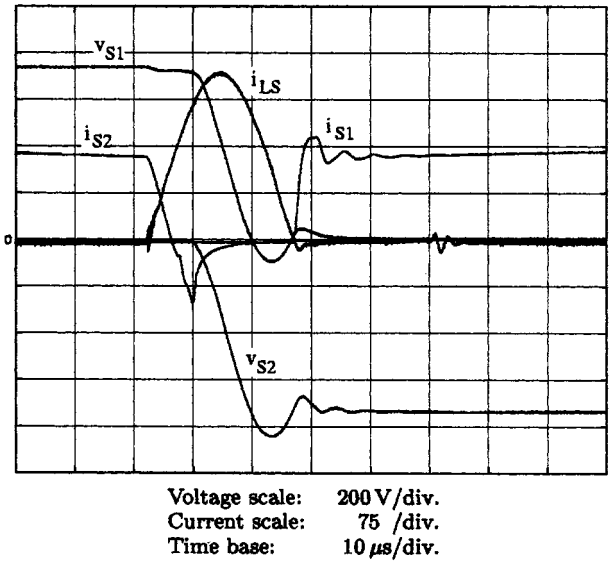

Fig. 9. Active commutation sequence: current boost mode.

this matter is that the lack of a series inductor does not constrain the application of the resonant snubbers with MTOs and possibly other thyristor-type devices with highly interdigitated gate–cathode structure. Low dI/dt rates result from the zero-voltage-switching (ZVS) conditions implying a reduction of the α of the transistors in the MTO structure (wide neutral region in the N-base at low voltages), resulting in a less intense regenerative action and slower turn-on process.

D. Active Commutation

The active commutation sequence preserves the turn-on characteristics observed in the analysis of the passive commutation sequence. The main difference between the turn-on processes in these two commutation sequences is the magnitude of the reverse voltage across the incoming switch, significantly lower in the active commutation case. The turn-off process, on the other hand, is unique due to its zero-current-switching (ZCS) nature and the effects of the charge stored in the outgoing switch over the commutation process.

The active commutation sequence starts as the snubber switch is turned on. Fig. 9 shows typical active commutation waveforms with the outgoing switch being turned-off under ZCS conditions. The switching conditions are such that $i_A \approx 150$ A, $v_{AK} = 750$ V, and $C_S = 1.0\ \mu$F.

1) Turn-Off Process Issues: Fig. 9 shows that the reverse-recovery waveforms are quite similar to the ones obtained for power thyristors. A difference is the presence of the antiparallel diodes in the turn-off MOSFETs, limiting the reverse voltage across the gate–cathode junction to about -1 V. The gate–cathode voltage changing from the forward voltage drop ($\approx$2 V) to the reverse clamp voltage causes the anode–cathode voltage to change by the same amount, resulting in transient current flow through the snubber capacitors.

TABLE III
ACTIVE COMMUTATION—TURN-OFF DATA

	C_S [μF]	1.0
	L_S [μH]	11.3
	i_{dc} [A]	136
	V_{in} [V]	750
Snubber	$i_{L_{S_{peak}}}$ [A]	277
	RMS factor [A$\sqrt{s}$]	0.95
Turn-off	E_{off} [mJ]	75
	$v_{AK_{max}}/V_{in}$	1.13
	di_A/dt [A/μs]	-36
	I_{rr} [A]	-102
	Q_{rr} [μC]	356
	t_{rr} [μs]	7.0
	Softness factor	0.52

The peak reverse recovery current I_{rr} and charge Q_{rr} under the conditions in Fig. 9 are listed in Table III, as well as other relevant turn-off data. Large reverse-recovery charge is observed in large devices such as the MTOs employed in this test setup. The reverse-recovery charge of the outgoing switch is used to boost i_{L_S} to the magnitude required to compensated for losses during the resonant mode and guarantee ZVS conditions for the incoming switch (snubber energy boost). The portion of the reverse-recovery current with positive derivative is associated with the turn-off losses in the outgoing switch, contributing to increase the losses during the resonant mode in the active commutation sequence.

The rms factor presented in Table III can be reduced to the classical definition of the rms value by multiplying the rms factor by $1/\sqrt{T}$, where T is the switching period. This definition allows prompt evaluation of the rms value of the snubber inductor current as well as the losses in the snubber inductor-switch branch for different switching frequencies.

2) Turn-On Process Issues: The switching conditions as well as relevant turn-on data are listed in Table IV. A comparison between the turn-on losses computed for the passive and active commutation indicate higher losses for the latter one, under about the same operating conditions. This fact can be explained from the shorter interval between the instant when the incoming device is gated on ($v_{AK} < 0$, $dv_{AK}/dt < 0$) and the instant where it starts conducting ($v_{AK} \approx 0$, $dv_{AK}/dt > 0$) in the active commutation sequence. The turn-on process is slowed down further due to the reduction of the charge injected into the P-base and N-base regions of the device, increasing the turn-on losses. The dI/dt associated with the turn-on process in the active commutation as well as the peak anode current relative to the dc-bus current are listed in Table IV.

IV. CONTROL CONSIDERATIONS

In order to guarantee ZVS for the incoming switch, it is required to boost the snubber energy at the beginning of the resonant mode. The minimum amount of energy boost corresponds

TABLE IV
ACTIVE COMMUTATION—TURN-ON DATA

	C_S [μF]	1.0
	L_S [μH]	11.3
	i_{dc} [A]	136
	V_{in} [V]	750
Snubber	$i_{Ls_{peak}}$ [A]	277
	RMS factor [A$\sqrt{s}$]	0.95
Turn-on	E_{on} [mJ]	35
	$i_{a_{max}}/i_{dc}$	1.25
	di_A/dt [A/μs]	109

to the losses associated with the resonant mode in the active commutation sequence. Two strategies to boost the snubber energy have been proposed in the literature: the current-boost and the voltage-boost approaches [2], [3].

The current-boost approach is based on delaying the instant where the outgoing switch is turned off ($t = t_o^c$), so that $i_{L_S}(t_o^c) > i_{\rm dc}$. The extra energy trapped in the snubber inductor at the beginning of the resonant mode corresponds to $(L_S I_{rr}^2)/2$ and it is strongly influenced by $i_{\rm dc}$, $i_{L_S}(t_o)$ and di_{L_S}/dt. This strategy has been employed throughout this paper and is illustrated in Fig. 9. The voltage boost approach is based on anticipating the turn-off instant of the outgoing switch $t = t_o^v$ in order to obtain $i_{L_S}(t_o^v) < i_{\rm dc}$. This condition results in boosting the snubber energy through an increase in the voltage on the snubber capacitors across the switches in the group undergoing commutation. An advantage of this latter strategy is the reduced dependence on the device Q_{rr}. Both snubber energy boost strategies can be obtained from the general solution for the resonant mode in the active commutation sequence [2]

$$\begin{aligned} v_{C_{S_n}}(t-t_o) = {} & Z_o[i_{dc} - i_{L_S}(t_o)] \sin \omega_o(t-t_o) \\ & + v_{L_S}(t_o) \cos \omega_o(t-t_o) \\ & - v_{L_S}(t_o) + v_{C_{S_n}}(t_o) \end{aligned} \tag{1}$$

$$\begin{aligned} i_{L_S}(t-t_o) = {} & \frac{1}{Z_o} v_{L_S}(t_o) \sin \omega_o(t-t_o) \\ & - [i_{\rm dc} - i_{L_S}(t_o)] \cos \omega_o(t-t_o) \\ & + i_{\rm dc} \end{aligned} \tag{2}$$

where $\omega_o = 1/\sqrt{L_S C_{S_{eq}}}$ and $Z_o = \sqrt{L_S/C_{S_{eq}}}$, $C_{S_{eq}} = 3C_S$ for three-phase realizations and $C_{S_{eq}} = 2C_S$ for the commutation cell.

A detailed view of the turn-off process associated with the voltage boost mode is shown in Fig. 10. As the outgoing device is turned off, the resonant mode is initiated. The voltage across both devices rise in the positive direction, increasing the energy in the snubber. As soon as the resonance brings the voltage on the outgoing device to negative levels, this device enters reverse conduction mode. The outgoing device continues in the reverse conduction mode until the excess carriers in junction j_1 are swept out by the reverse anode current. The gate–cathode junction does not enter avalanche breakdown due to the presence of the reverse diodes in the turn-off MOSFETs.

Large power devices always undergo a reverse-recovery process in the active commutation sequence, independent of the turn-off method employed. This statement holds true for any design of the resonant snubbers of practical interest. Also, the relatively large switching times of large devices introduce additional uncertainty in the computation of the gate turn-off point leading to the desired snubber energy boost. In fact, the low dI/dt at gate turn-off shown Fig. 10 implies that a nonnegligible amount of energy is dissipated instead of transferred to the snubber capacitors. These characteristics make the snubber current boost preferable when large, slow devices are employed in the main converter switches.

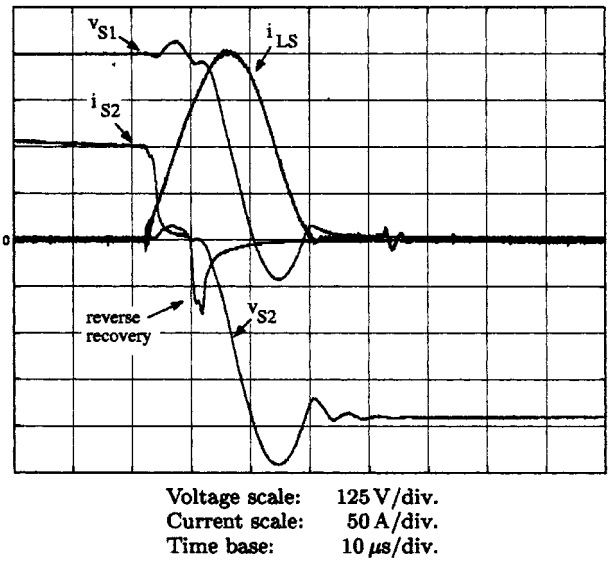

Fig. 10. Active commutation waveforms: snubber voltage boost.

V. TRADEOFF IN THE DESIGN OF THE RESONANT SNUBBERS FOR CSCS

A. Design of the Snubber Capacitor C_S

The critical dV/dt rating of the device employed in the main switches (rated at 1000 V/μs for the MTO employed in this work) along with the maximum dc-bus current defines a theoretical minimum size for the snubber capacitors. This rating, however, is generally related to the maximum dV/dt the device could be subjected to without retriggering. A more restrictive constraint is introduced by the reduction of the switching losses, typically leading to capacitor sizes larger than those obtained from the critical dV/dt.

The minimum snubber capacitor size is set by the upper limit established for the turn-off energy loss during the passive commutation process. This reduction on the turn-off losses is obtained from the reduction of the dV/dt across the outgoing switch, lengthening the passive commutation interval for a given dc bus current. Detrimental effects of long commutation intervals include limitation of the PWM frequency and distortion of the ac waveforms, from comparatively large dwell times. Proper design of the snubber capacitor requires the use of experimental data relating the turn-off losses with the size of the snubber capacitor for given conditions of dc-bus current and input voltage. Models approximating the turn-off characteristic of GTOs have been proposed in the literature [5]

and can certainly be extended for MTOs given the similarities between these devices.

The placement of the snubber capacitor directly across the terminals of the power device introduces a second path for the current during the forward recovery process. As the forward voltage drop across the incoming device increases, due to the high device impedance in the initial stages of the turn-on process, the voltage across the snubber capacitor also increases. During this interval, part of the dc-bus current is diverted through the snubber capacitor. The resultant reduction of the magnitude of the current injected in the device during the initial stages of the forward recovery process contributes to augment the duration of this transient and to reduce the dI/dt at turn-on. As the impedance of the device drops rapidly causing v_{AK} to drop to the steady-state conduction level (conductivity modulation), the snubber capacitor discharge through the incoming device. The effects are an increase in the turn-on losses and current overshoot.

B. Design of the Snubber Inductor L_S

The snubber inductor design is aimed at the active commutation sequence. The basic design goal is to guarantee ZVS conditions for the incoming switch with minimum voltage and current stress on the main converter switches and snubber components.

The reverse recovery characteristics of the main power devices have significant impact on the performance of the resonant snubber. When the outgoing switch is turned off in ZCS mode, the snubber inductor current i_{L_S} is boosted by a magnitude corresponding to I_{rr}, increasing the energy stored in L_S. However, excessive boost of the snubber energy leads to higher voltage stress as the voltage on the snubber capacitor across the outgoing device is driven beyond the input voltage level. Fig. 11 shows computed plots of the extra voltage stress on the main switches as a function of the characteristic impedance Z_o of the resonant snubber for several values of I_{rr}. Low values of characteristic impedance are required to limit the overvoltage across the main switches. However, a reduction of the snubber inductor size increases the turn-off dI/dt (for a given input voltage), leading to larger I_{rr} and higher voltage and current stresses.

In this analysis, the base values are: $V_{\text{base}} = V_{L,\text{RMS}}$, $I_{\text{base}} = I_{L,\text{RMS}}$ and $Z_{\text{base}} = V_{\text{base}}/\sqrt{3}I_{\text{base}}$. The input voltage and dc-bus current are assumed at maximum values for the purpose of stress estimation ($V_{\text{in}} = \sqrt{2}$ pu, $i_{\text{dc}} = \sqrt{2}$ pu). The estimates in Fig. 11 are conservative since all losses were neglected.

Equally important as design quantities are the rms and peak current levels through L_S. Since the snubber inductor and switch are series connected, the current through L_S also determines the current carrying characteristics required for the snubber switch Th_S. Here, the goal is to minimize the peak current through the snubber inductor relative to the dc-bus current. The peak value of the snubber inductor current $i_{L_S,\max}$ is reached during the resonant mode. From (3) $i_{L_S,\max}$ is computed as

$$i_{L_S,\max} = \sqrt{\left(\frac{v_{L_S}(t_o)}{Z_o}\right)^2 + I_{rr}^2} + i_{\text{dc}}. \tag{3}$$

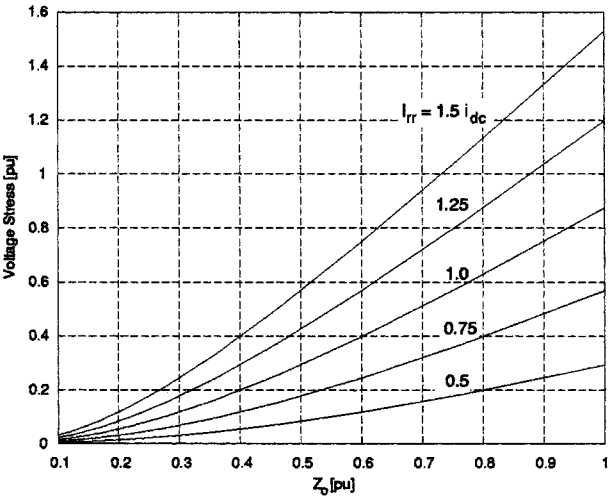

Fig. 11. Active commutation: voltage stress due to large I_{rr}.

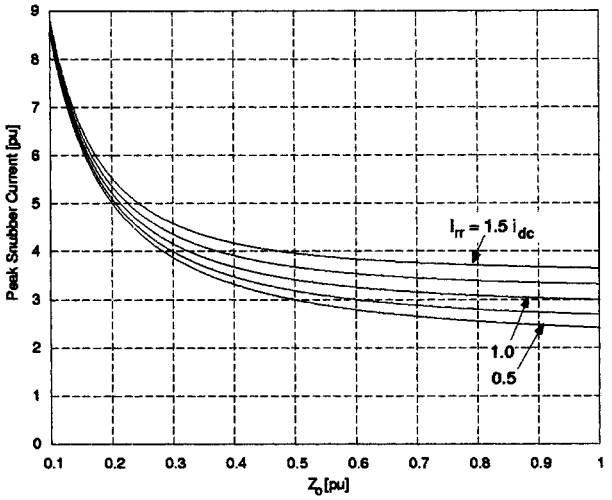

Fig. 12. Active commutation: current stress due to large I_{rr}.

Fig. 12 illustrates the dependence of the peak snubber current on Z_o, for the same conditions employed in Fig. 11. From Fig. 12, it is clear that a compromise between the magnitude of the current through L_S and, consequently, the losses on the snubber components, and the extra voltage stress on the main switches has to be established.

The turn-off loss on the outgoing switch is also a factor to be included in the design of L_S. From Fig. 9, it is seen that the voltage across the outgoing switch is reapplied during the resonant mode in the active commutation process. The rate of decay of the reverse recovery current is determined by recombination inside this device as well as the formation of the depletion region. The reapplied dV/dt can be controlled through the natural resonance frequency of the snubber ω_o. Low values of ω_o are desirable to reduce the turn-off losses, but the commutation interval should be kept short for higher switching frequency capability.

VI. Conclusion

The impact of the switching characteristics of high-power devices compatible with medium-voltage CSC applications on the

resonant snubber design and performance has been addressed in this paper.

A closer look into the MTO turn-off process reveals some limitations, mainly in hybrid devices: high sensitivity to stray inductances in series with the MOSFETs, intrinsic limit on the maximum anode current that can be turned off, and potential for uneven current distribution at turn-off. These characteristics imply the use of turn-off snubbers across the MTOs. In the test setup, the rate of reapplied voltage has been limited to 100 V/μs. Attempts to turn off the devices at higher dv_{AK}/dt rates resulted in device failure at relatively modest current and voltage levels (200 A/600 V). Possible causes for turn-off failure include: retrigger during the thyristor phase in the turn-off process, second breakdown, and uneven pressure distribution over the device surface. These results are not inconsistent with the dv_{AK}/dt rating from the device data sheet (1000 V/μs @ $V_D = 0.7\ V_{DRM}$, $G_2 = +15$ V), since this rating is given for steady-state blocking mode. Further investigation is still needed for a complete characterization of the MTO turn-off performance.

The MTOs were observed to exhibit self-limited dI/dt at turn-on. In addition, the ZVS conditions contribute to slow down the turn-on process, reducing the current transfer ratio α of the transistors in the device structure ($di_A/dt < 200$ A/μs for dc-bus currents up to 200 A). The trigger timing and reverse-recovery characteristics of the main switches have been identified as important manipulation and disturbance quantities in the control of the commutation processes of the resonant snubber.

REFERENCES

[1] W. McMurray, "Resonant snubbers with auxiliary switches," *IEEE Trans. Ind. Applicat.*, vol. 29, pp. 355–361, Mar./Apr. 1993.

[2] B. J. Cardoso and T. A. Lipo, "Current stiff converter topologies with resonant snubbers," in *Conf. Rec. IEEE-IAS Annu. Meeting*, New Orleans, LA, Oct. 1997, pp. 1322–1329.

[3] ——, "A reduced parts count realization of the resonant snubbers for high power current stiff converters," in *Proc. IEEE APEC'98*, Los Angeles, CA, Mar. 1998, pp. 558–564.

[4] B. J. Cardoso, S. Bernet, and T. A. Lipo, "A new control strategy for the PWM current stiff rectifier/inverter with resonant snubbers," in *Proc. IEEE PESC'97*, St. Louis, MO, June 1997, pp. 573–579.

[5] H. Ohashi, "Snubber circuit for high power gate turn-off thyristor," *IEEE Trans. Ind. Applicat.*, vol. 19, pp. 655–664, July/Aug. 1983.

[6] J. Holtz, M. Stamm, J. Thur, and A. Linder, "High-power pulsewidth controlled current source GTO inverter for high switching frequency," in *Conf. Rec. IEEE-IAS Annu. Meeting*, New Orleans, LA, Oct. 1997, pp. 1330–1335.

[7] D. E. Piccone, R. W. DeDoncker, J. A. Barrow, and W. H. Tobin, "The MTO thyristor—A new high power bipolar MOS thyristor," in *Conf. Rec. IEEE-IAS Annu. Meeting*, Oct. 1996, pp. 1472–1473.

[8] D. E. Piccone *et al.*, "MTO thyristor," SPCO, Exton, PA, Application Notes, Fall 1997.

[9] B. J. Baliga, *Power Semiconductor Devices*. Boston, MA: PWS, 1996.

[10] R. Rodrigues, D. Piccone, A. Huang, and R. DeDoncker, "MTO thyristor power switches," in *Conf. Rec. Power Systems World*, Baltimore, MD, Sept. 1997, pp. 3.53–3.64.

[11] D. F. Grafham and F. B. Golden, *SCR Manual Including Triacs and Other Thyristors*. Englewood Cliffs, NJ: Reward Books, 1979.

[12] R. W. DeDoncker and J. P. Lyons, "The auxiliary resonant commutated pole converter," in *Conf. Rec. IEEE-IAS Annu. Meeting*, Oct. 1990, pp. 1228–1235.

[13] G. L. Skibinski and D. M. Divan, "Characterization of GTO for soft switching applications," in *Conf. Rec. IEEE-IAS Annu. Meeting*, Oct. 1988, pp. 638–646.

[14] P. Wood, *Fundamentals and Applications of Gate-Turn-Off Thyristors*. Palo Alto, CA: EPRI, 1988.

Braz J. Cardoso Filho (S'95–M'98) was born in Fortaleza, Brazil. He received the electrical engineering (with the EEUFMG Lucio dos Santos Award) and Master of electrical engineering degrees from the Universidade Federal de Minas Gerais, Belo Horizonte, Brazil, and the Ph.D. degree from the University of Wisconsin, Madison, in 1987, 1991, and 1998, respectively.

In 1989, he joined the Department of Electrical Engineering, Universidade Federal de Minas Gerais, where he became an Associate Professor in 1998. He has developed research and teaching activities in the power electronics area since 1988. His current research interests are power semiconductor devices, multimegawatt converters, electric drive systems, and utility applications of power electronics.

Thomas A. Lipo (M'64–SM'71–F'87) is a native of Milwaukee, WI. He received the B.E.E. and the M.S.E.E. degrees from Marquette University, Milwaukee, WI, in 1962 and 1964, respectively, and the Ph.D. degree in electrical engineering from the University of Wisconsin, Madison, in 1968.

From 1969 to 1979, he was an Electrical Engineer in the Power Electronics Laboratory of Corporate Research and Development, General Electric Company, Schenectady, NY. He became a Professor of Electrical Engineering at Purdue University, West Lafayette, IN, in 1979 and, in 1981, he joined the University of Wisconsin, Madison, in the same capacity. He is presently the W. W. Grainger Professor for Power Electronics and Electrical Machines, Co-Director of the Wisconsin Electrical Machines and Power Electronics Consortium, and Director of the Wisconsin Power Electronics Research Center.

Dr. Lipo has received the Outstanding Achievement Award from the IEEE Industry Applications Society, the William E. Newell Award from the IEEE Power Electronics Society, and the 1995 Nicola Tesla IEEE Field Award from the IEEE Power Engineering Society for his work. Over the past 30 years, he has served the IEEE in numerous capacities, including President of the IEEE Industry Applications Society.